Nano LIFE
Vol. 13, No. 4 (2023) 2350014 (13 pages)

DOI: 10.1142/S1793984423500149

World Scientific
www.worldscientific.com

Exploiting the Electrical Nature of Biofilms for Long-Term Monitoring of Quiescent Aquatic Environments via Open-Circuit Microbial Potentiometric Sensors: Evidence of Long-Distance Electrical Signaling

Scott R. Burge*, Kiril D. Hristovski[†,¶], Russell G. Burge*, Ljupco Pejov[†,‡], Dragan Boscovic[§], Evan Taylor* and David A. Hoffman*
[*]*Burge Environmental Inc., 6100 South Maple Avenue, Tempe, Arizona 85283, USA*
[†]*Environmental and Resource Management, The Polytechnic School, Ira A. Fulton Schools of Engineering, Arizona State University, Mesa, Arizona 85281, USA*
[‡]*Institute of Chemistry, University of Ss. Cyril and Methodius, Skopje 1000, North Macedonia*
[§]*School of Computing and Augmented Intelligence, Ira A. Fulton Schools of Engineering Arizona State University, Tempe, Arizona 85281, USA*
[¶]*kiril.hristovski@asu.edu*

Received 12 September 2023
Accepted 28 September 2023
Published 8 November 2023

This study was based on the hypothesis that spatial–temporal characterization of contaminant-affected redox gradients in a quiescent system could be measured by microbial potentiometric sensor (MPS) arrays incorporated in large, natural biofilm networks. Two experimental chambers, each containing at least 48 equidistantly located MPS electrodes, were fabricated to examine reproducibility of the patterns. The MPS electrodes were exposed to biofilm growth conditions by introducing high dissolved organic carbon (DOC) and dechlorinated tap water at the bottom of the experimental chamber; and the spatial–temporal changes in the MPS array signals were recorded, which showed that signal trends were correlated to the induced changes in DOC. The results indicated that MPS arrays measured the spatial–temporal changes in the aqueous solution caused by an influx of carbon rich water, which could not be detected by conventional oxidation-reduction potential (ORP) electrodes. Interestingly, the experiments conducted over long time periods revealed unusual behaviors like electrical signaling and possible potentiometrically driven communication within the biofilm. These observed behaviors suggest that biofilms may create a large network through which communication signals can be generated and propagated by inducing changes in electric potentials similar to a sophisticated electronic device.

Keywords: sensor, biofilm, monitoring, signaling, electrical

[¶]Corresponding author.

1. Introduction

Commonly used descriptions in the literature describe biofilms as consortia of different microorganisms organized in a communal structure, which promotes symbiotic functions and protection against adverse external influences.[1–3] In a broader sense, however, biofilms have many of the characteristics of a primitive lifeform that is capable of interacting with the surrounding environment and communicating information throughout the biofilm structure and microorganisms.[4,5] Chemical communication among the different cells within a biofilm has been documented in the literature.[1–5] Recent evidence suggests that biofilm microorganisms may be capable of communicating via electrical signaling pathways using cytochromes and specialized nanosized organelles to transfer charge and thus information within and beyond the biofilm boundary.[6–8]

Much of the evidence suggesting electrical or electrochemical communication originates from the work conducted on fuel cell technology, which explores electrochemically active biofilms.[9–16] These biofilms can funnel the excess electrons to an electrode, while protons flux out of the biofilm.[17–21] The overall electron fluxes could be generally organized into two categories: Soluble electron transfers and bound electron transfers. Soluble electron transfers could be envisioned as electrons exchanged between the solution and the biofilm surface.[22] In contrast, bound electron transfers are modeled as electrons exchanged in the biofilm matrix or at the cell membrane.[23–25] The magnitude of these electron fluxes correlates strictly with the metabolic processes of the biofilm.[26–30] Regardless of the specific types of metabolic and electron transfer pathways, the overall electron fluxes control the establishing of electric potential gradients on a microscale (or even nanoscale) as determined by the local redox and nutrient conditions.[31–33]

Under equilibrium conditions, a steady state exists between the soluble electron transfers and bound electron transfers, which is characterized by a steady-state open-circuit electric potential.[34–36] Because no electric current is flowing in an open-circuit system, the electric potential is precisely dependent on the local equilibrium conditions that are driven by both the biochemical processes in the biofilm and the redox conditions outside the biofilm, such as nutrient concentration.[26–33] Any biochemical changes in the local environment surrounding the biofilm will inherently induce changes in the biochemical rates and types of processes within the biofilm, which will change the open-circuit potential (OCP). Such biochemical changes in the local environment cannot be readily detected by the oxidation-reduction potential (ORP) sensors, which represent the golden standard in measuring the oxidizing and reducing conditions in water bodies.[37,38] Although the ORP sensors measure open-circuit potential, this golden standard is flawed when it comes to long-term measurements of naturally existing water matrices, which exhibit heterogeneous redox conditions and may require high activation energies for redox reactions or dilute concentrations of redox species.[39]

In a closed-circuit scenario, like in a fuel cell, an induced electric current is flowing through the biofilms enabling them to transfer the electrons to a preferential electron acceptor (typically oxygen), which is kept at a gradient to maximize the flow of electrons.[40–42] While closed-circuit scenarios create a steady-state flow of electrons, this electron flow does not reflect the normal metabolic pathways that are typical of equilibrium conditions.[34–36] This flow of electrical current deviates the system from its normal metabolic paradigm, so it no longer describes the state of the natural, endemic biofilm, which proliferates in undisturbed local redox and nutrient conditions. As such, using a closed-circuit approach to monitor biofilm behavior and correlating that behavior to comprehensively understand biofilms and their local environments has limitations because it does not permit observing behavior in normal equilibrium conditions, and thus is a representative of the natural processes (e.g., exoelectrogens proliferation increased compared to undisturbed conditions). In brief, closed-circuit approaches do not enable observation of biofilm behavior under equilibrium conditions, which represent the most prevalent scenarios in a life of a biofilm. Similar to Heisenberg's Uncertainty Principle, one cannot observe a system in a natural state when the natural state is disturbed by the observation tool. By inducing a flow of electric current to observe the biofilm behavior, one is disturbing the natural state of the biofilm. The subsequent question then becomes how can one observe the behavior of biofilms without changing the system or their natural states. Developing

such a tool or methodology has the potential to open new perspectives on understanding how biofilms communicate and interact with their local environment.

In this study, we propose an alternative approach to monitoring the behavior of biofilms via an open-circuit method. Monitoring of the behavior of a biofilm and its local environment with an open-circuit approach eliminates the drawbacks associated with inducing external changes in the bioelectrochemistry of the biofilm and enables temporal characterization of a system undisturbed by a flow of externally introduced electrons. Consequently, all the changes in the electric potential are directly related only to the local environmental conditions and the biofilm characteristics and its biochemical processes.

Figure 1 illustrates a simplified depiction of an open-circuit measurement sensor array through which the electric potentials of biofilms can be measured. Rooted in simple electronics, the open-circuit system comprises a reference electrode (an electrode with a constant electric potential (e.g., Ag/AgCl reference electrode) and an electrode comprising a nonoxidizable conductive surface upon which endemic microorganisms can establish biofilm populations. The two electrodes are connected to high impedance (> 1 GΩ) measurement circuitry capable of measuring OCP (voltage). Because OCPs are measured, multiple biofilm electrodes (an array) could be referenced against a single reference electrode.[43] The described open-circuit measurement system is dubbed microbial potentiometric sensor (MPS) system because the biofilm microorganisms represent the actual electrode whose OCP is measured against the reference electrode.

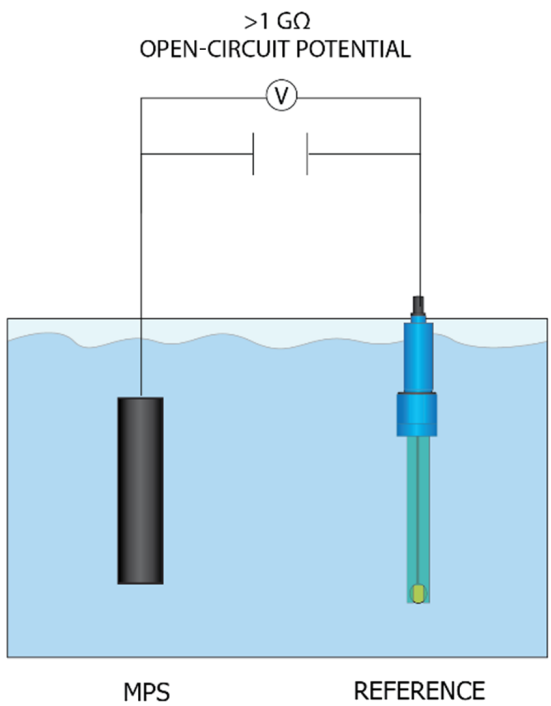

Fig. 1. Simplified depiction of an OCP measurement system (microbial potentiometric electrode and reference electrodes) connected to a high impedance OCP measuring device.

Considering the advantage of using a single reference, an MPS array system comprising multiple biofilm electrodes, which are placed at different locations through an environmental system, can be used to provide real-time spatial–temporal monitoring and visualization of contaminant mass transport or other changes in quiescent systems.[38,39,44–47] Consequently, an overarching hypothesis was postulated that spatial–temporal characterization of contaminant affected redox gradients in a quiescent system could be obtained by creating an MPS array system comprising multiple equidistant biofilm electrodes.

To validate the hypothesis, four task-oriented objectives were completed. Specifically, two experimental chambers, each containing at least 48 equidistantly located MPS electrodes, were fabricated to examine reproducibility of the patterns. The MPS electrodes were exposed to biofilm growth conditions and monitored following a methodology described by Burge *et al.*[38] Upon biofilm growth stabilization, the experimental chambers were filled with dechlorinated tap water and monitoring of the MPS potentials was conducted by introducing high dissolved organic carbon (DOC) and dechlorinated tap water at the bottom of the experimental chamber. Spatial–temporal changes in the MPS array signals were recorded and signal trends were correlated to the induced changes in DOC water quality.

2. Methodology

2.1. *Fabrication of experimental chambers and biofilm growth*

Two experimental chambers were fabricated for the purposes of this study. As illustrated in Fig. 2, the experimental chambers were fabricated using

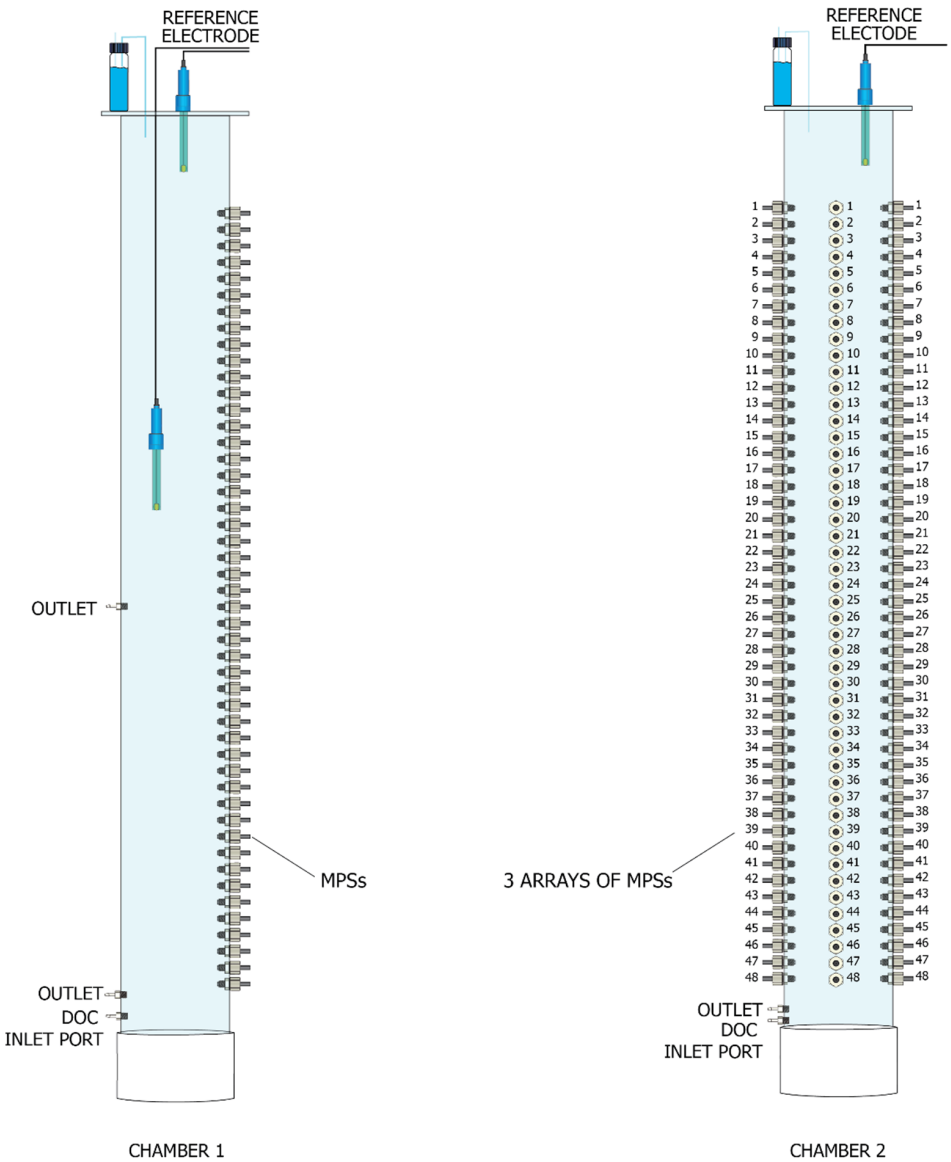

Fig. 2. Schematic representations of the chamber arrays containing 48 MPS electrodes (left) and 3 × 48 MPS (right) electrodes, respectively.

clear polycarbonate tubes with inner diameter of $d_I = 15.25$ cm and length of $l = 152$ cm. These vertically orientated chambers were sealed at the bottom and the top, with the top containing ports enabling exchange with atmospheric oxygen as needed. Ports were fabricated at several vertical locations along the wall of the chambers to enable introduction and removal of solutions. The total volume of the chambers was 28.1 L.

Each chamber contained a vertical array of 48 graphite (MPS) electrodes with diameter of $d_E = 0.64$ cm mounted in a PVC threaded fitting. The MPS electrodes were spaced at 1 inch (2.54 cm) center-to-center distance from each other. The surface of the graphite rod exposed to the environment was flush with the terminal end of the fitting and enabled sufficient surface for biofilm proliferation.[38] The opposite end of the graphite electrode was fitted with an electrical wire/cabling for connection with the signal acquisition tools. An Ag/AgCl electrode was placed on the top of each chamber so as to serve as a reference for the MPS electrodes.

Chambers 1 and 2 were fabricated identically to examine data reproducibility and repeatability, except that chamber 2 comprised 144 MPS sensors

in three vertical arrays, organized in the same equidistance pattern as experimental chamber 1, to examine variability of the sensor signal at the same height. The three sensors located at the same height were located at 90° angles from each other as illustrated in Fig. 2. Additionally, chamber 1 contained three ORP electrodes located at 30 cm, 67.5 cm and 95 cm below the top of the chamber. Chamber 2 contained two ORP electrodes. The ORP electrodes were installed in the systems to observe if there are any deviations in signal difference between the ORP and the MPS sensors as the experimental conditions changed.

To initiate biofilm growth, the chambers were filled with dechlorinated tap water (City of Tempe) and kept at temperature of $T = 24 \pm 1$°C in the dark to prevent the development of any photosynthetic microorganisms. The system was left undisturbed for a period of several weeks to promote biofilm development on the graphite electrode surfaces. The OCP signals from each MPS electrode were measured against the reference electrode at least once a day with a high-impedance voltmeter (>1 GΩ). The biofilm development on the electrodes was considered complete once the signals were stable, exhibiting signal variability of ± 3 mV between daily measurements.

2.2. *Spatial–temporal monitoring of the MPS potentials under high DOC and dechlorinated tap water conditions*

Chamber 1. Upon completion of the biofilm stabilization period, chamber 1 was filled with dechlorinated water, and anaerobic water (DOC > 100 mg/L) was slowly gravity-fed through a port located at the bottom of the chamber at a rate of 450 ± 150 mL/day. This rate of anaerobic water introduction allowed the visual observation of the interface between the dark brown anaerobic solution and the overlying clear water. Once the anaerobic water reached a height between MPS 40 and MPS 41, the introduction of the anaerobic water was stopped and ORP electrodes were installed. The ORP electrodes were installed later to minimize the disruption of any diffusive processes by a free hanging electrode during the high DOC water injection period. The chamber was left undisturbed and exposed to atmospheric air for a period of approximately four months to monitor any changes resulting from oxygen diffusion. After this period, the chamber was sealed off to eliminate any atmospheric influences. Any headspace was removed by adding < 1 L aerobic (atmospheric oxygen containing) water. The monitoring of chamber 1 was continued for a period of six months before the experiment was terminated. Three months after the capping, a small pinhole opening in the system was created that enabled small diffusion of oxygen.

Chamber 2. To validate the observations from chamber 1 and obtain better understanding of the spatial variability of the signals, chamber 2 was constructed with three times more sensors allowing for examination of the horizontal changes in the OCPs. Upon completion of biofilm stabilization and the conditioning period, anaerobic water was slowly gravity-fed through a port located at the bottom of the chamber at a rate of 600 ± 100 mL/day until the anaerobic water interface solution reached MPS 34. Approximately two weeks later, the column was bleached three times (using a 1% bleach solution) and rinsed with tap water before filling the chamber with aerobic water. Four days after filling the chamber with aerobic water, aerobic water was introduced through the bottom port at the same rate. Once the anaerobic water interface reached the height between MPS 30 and MPS 31, the introduction of anaerobic water was terminated and the ORP electrodes were installed. The chamber was left undisturbed and exposed to atmospheric air for a period of about three months. The chamber was then capped and any headspace was removed by adding < 1 L aerobic water, so that no atmospheric oxygen could enter the system until the experiment was completed several days later.

3. Results and Discussion

3.1. *Spatial–temporal monitoring of the MPS potentials in Chamber 1*

Figure 3 illustrates the average OCPs for several nine-consecutive-day durations as generated by each of the 48 MPS sensors against the reference electrode. Only periods 1, 2, 3 and 9 are illustrated in Fig. 3(a) to minimize the data crowding in this figure (Figs. S1 and S2 contain the additional seven nine-day periods). Period 1 illustrates the OCP

pattern generated by the MPS sensors before the injection of high DOC water. During this period, the signals generated by each MPS sensor were very stable as characterized by very small 95% confidence intervals of ~1 mV. However, once the high DOC water was introduced (period 2), the stability of each of the 48 MPS sensors decreased as their OCPs started declining. Interestingly, the introduction of the high DOC water caused unexpected drop in potential of almost all MPS sensors, and not only of the MPS sensors located near the bottom of the chamber where the high DOC water was introduced. While the OCP changes in MPS sensors located near the injection port where the high DOC water was introduced were expected, they could not only be attributed to the diffusion of the DOC. Diffusion of the DOC from the bottom upwards was slow and created a clear potential gradient slowly moving from the bottom up as evidenced in Fig. 3(a); these gradients in potential cannot be explained if only diffusion was at work. By the end of period 7, most of the sensors above the visible gradient boundary between MPS 40 and MPS 41 responded to the change in OCP corresponding to high DOC, for example, the biofilm in the sensors near the bottom of the chamber was communicating an electrical information about an incoming influx of DOC. Interestingly, not all MPS sensors above the DOC gradient boundary responded equally. Some exhibited a greater change in their OCP, and some hardly changed as illustrated in OCP change and the depicted 95% confidence intervals.

When the introduction of the high DOC water ceased and oxygen was allowed to diffuse from the top, the OCP of all MPS sensors started increasing, which was followed by the shifting of the entire pattern of the potential gradient vertically upward

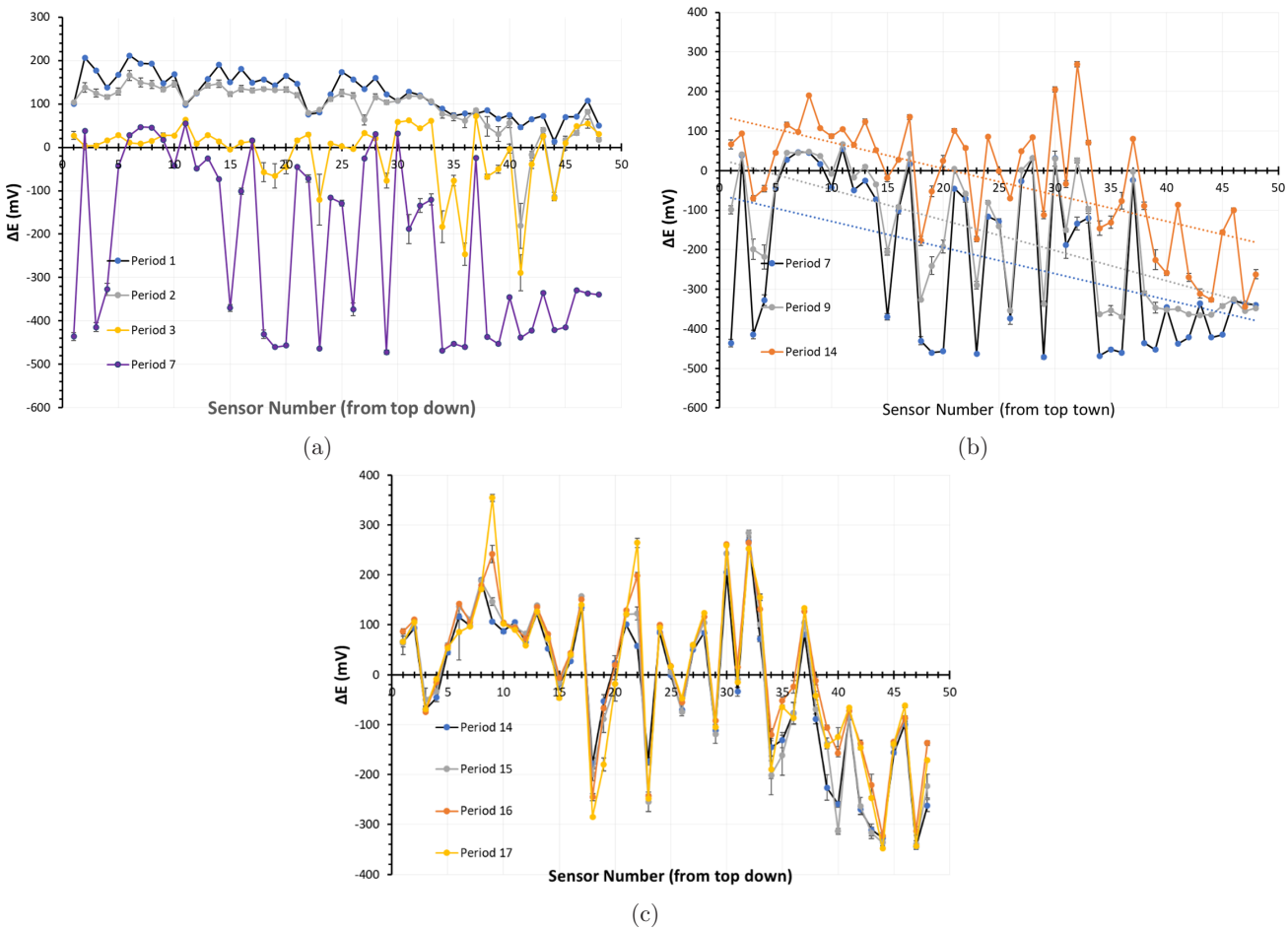

Fig.3. The average OCPs for several 17 periods as generated by each of the 48 MPS sensors in chamber 1 against the reference electrode. Each period consists of 9 ± 1 days. The error bars represent 95% confidence intervals. The dotted lines illustrate the linear trend illustrating the overall charge gradient in the system shifting up with respect to time.

in the chamber as illustrated in Fig. 3(b). The form of the pattern, however, maintained its general shape as the oxygen could enter and diffuse the column from the end of period 7 to the end of period 14. When the chamber was capped at the top to prevent diffusion of oxygen, the changes in the OCP in all MPS sensors started decreasing and eventually stopped by the end of periods 16 and 17 as illustrated in Fig. 3(c). This behavior was expected considering that additional oxygen was prevented from entering the system, which led to the microorganisms in the chamber (both biofilm and solubilized) to utilize the remaining dissolved oxygen and stabilize the redox potentials. This type of behavior implies that microorganisms in biofilms may be able to temporarily store the potential energy of the electrons, generated from the biochemical decomposition of organic carbon, in their networks of temporary electron acceptors when the energy harnessing conditions are unfavorable, and release them under more favorable conditions when the electron acceptor is present, which could provide with more energy. In brief, when oxygen is present, the microorganisms could extract most of the energy from the carbon; however, if oxygen is not present, they may decide to store the electrons by conserving their potential energy in the temporary electron acceptors, which would manifest the exhibited patterns.

The temporal changes in the overall bioelectrochemical conditions of the system during these 17 periods are illustrated in Fig. 4 which shows the daily changes of the average OCP in the chamber as detected by the 48 MPS sensors referenced against the Ag/AgCl electrode. The average OCP in the system decreased when the introduction of high DOC water commenced. Interestingly, however, the average OCP continued to decrease until it reached a minimum approximately 900 h after the injection had stopped. Once the minimum was reached, the ORP sensors were introduced, which showed stable but highly reducing conditions with an average ORP < -430 mV. As the average MPS potential started to increase, the ORP stayed relatively stable at < -430 mV for another 400 h, and then exhibited severe electric potential fluctuations, which stopped shortly after the chamber was capped. The MPS sensors detected the chamber capping by registering a small signal "dip" in the average signal. Once the chamber was capped, the ORP fluctuation subsided and the ORP remained generally < -400 mV regardless of the changes exhibited in the average MPS OCP. In contrast, the average MPS OCP stabilized and

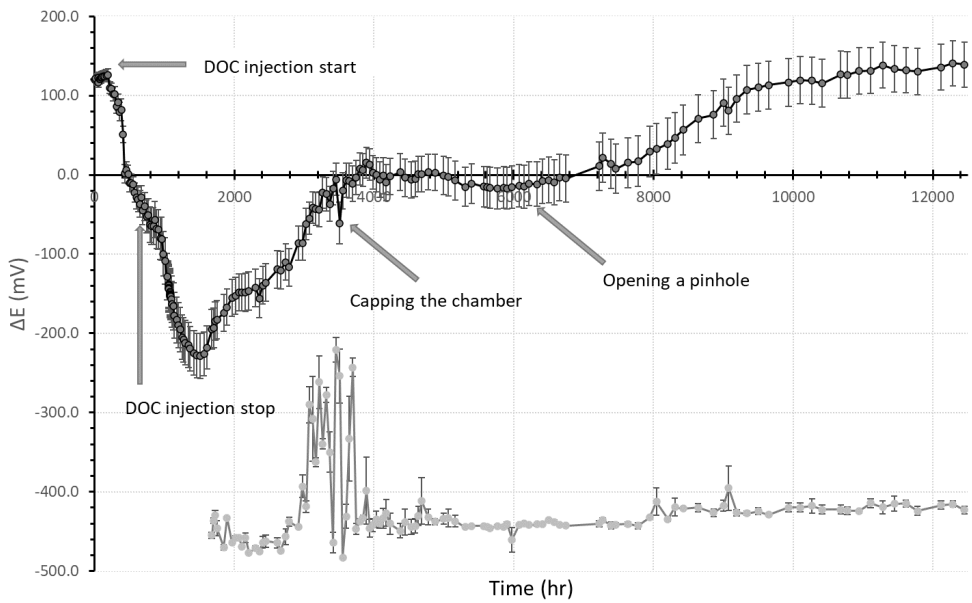

Fig. 4. Temporal changes in the overall bio-electrochemical conditions of the system during these 17 periods. Each data point represents an average of all the MPS or ORP generated OCP signals. Black symbols represent the average OCP signals from the 48 MPS electrodes in chamber 1. The gray symbols represent the average signals from the three ORP electrodes. The error bars represent 95% confidence intervals.

remained relatively stable for over 2000 h after the capping with a slight decreasing tendency as illustrated in Fig. 4. Once the pinhole was created, the miniscule amount of diffusive atmospheric gas (oxygen) caused the average MPS OCP to start slowly increasing until it reached the levels at the beginning of the experiment at $t > 12\,000$ h.

3.2. *Spatial–temporal monitoring of the MPS potentials in Chamber 2*

Figure 5(a) illustrates the overall bioelectrochemical conditions of the system during a period of over 4000 h as revealed by the OCPs of the three different columns, each containing 48 sensors. Once the system was stabilized as shown in Video 1 (Supplemental Materials), the average OCPs of columns did not deviate from each other. The average value for each column was < 15 mV and 95% confidence intervals showed that there is no statistical difference among the average values. The variance, as depicted through the 95% confidence intervals, started to increase as more high DOC water was introduced at the bottom of the chamber. This was expected considering that the sensors at the bottom started to identically respond to the presence of high DOC and created a well-defined gradient

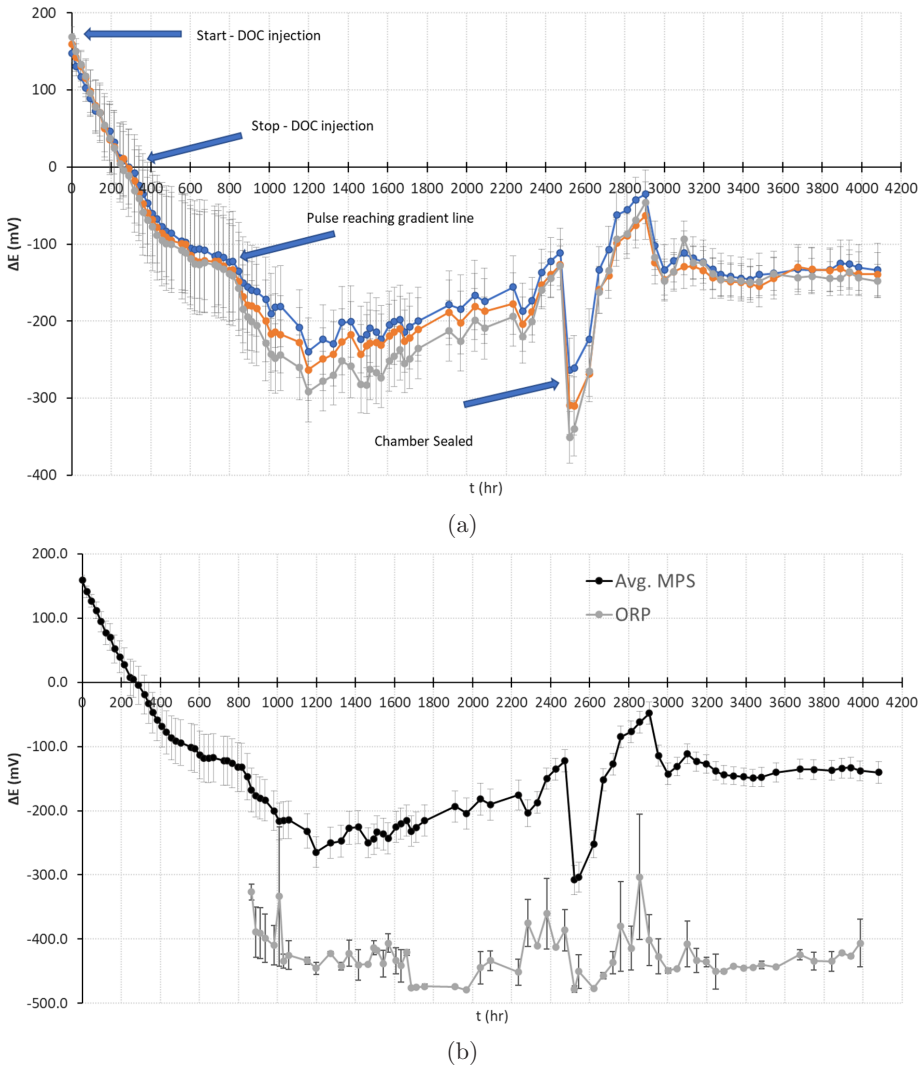

Fig. 5. Temporal changes in the overall bio-electrochemical conditions of the system during a period of $t > 4000$ h. (a) Each color represents the average signals from one of the three vertical arrays comprising 48 sensors in chamber 2. (b) Each data point represents an average of all the MPS or ORP generated OCP signals. Black symbols represent the average OCP signals from the 144 MPS electrodes in chamber 2. The gray symbols represent the average signals from the three ORP electrodes. The error bars represent 95% confidence intervals.

that reflected the DOC influx. This is well illustrated in Video 2 (Supplemental Materials), where the stability of the sensors and change of the OCP with the incoming flux is shown through time. At time $t \approx 318$ h, the injection of high DOC water was stopped, and the system stabilized as a result of which each sensor showed very little divergence from the main signal trend. Interestingly, however, a specific pulse is registered by all the MPSs near the bottom as illustrated in Video 2. The pulse is characterized by ~ 50 mV drop in the potential, and it subsequently moved up toward the gradient, although the high DOC water injection was terminated. All MPSs at a specific height generated OCP signals in concert. Apparently, the MPSs at the bottom were sending an electrical signal that the influx of high DOC water was terminated, and the system needed to readjust. This behavior could not be attributed to diffusion because diffusion would have already perturbed the established gradient characterized by a difference of about 400 mV. The upward movement of this pulse is also evident in Fig. 4, where a decrease in the average OCP continued to occur after the DOC injection had stopped. As more and more sensors from the bottom register the pulse, the average OCP signal variance increases, which is illustrated through the increasing 95% confidence intervals. The extensive overlap of these intervals shows that the probability of the average OCP signals being statistically different is significantly lower than 5%.

At $t \approx 815$ h, the pulse reaches the already established gradient, which causes the entire signal pattern to start shifting down. It appears like the pulse reached its designated destination and signaled the system to start decreasing its overall bio-electrochemical potential above the established ~ 400 mV gradient, while the shape of the pattern remains the same. This behavior could not be attributed to any bulk mass transport mechanism because there was no advective transport of DOC; and diffusion would not cause translational movement without changing the shape of the pattern. While it is documented that biofilms use nanovesicles to communicate and signal across distances, these represent mass transport mechanisms occurring over short distances.[48–54] Here, the communication occurred across distances exceeding 0.6 m and was exhibited by all sensors located at corresponding levels. Logically, there must have been a different mechanism that induced this type of behavior. Considering the velocity of signaling across all sensors, the nature of the signal (e.g., voltage), and the distance involved, it could be postulated that the pulse signal was electrical in nature. If so, this signal could only travel at this speed and distance only if there is some kind of interconnected network that enabled rapid transfer of electrons. If such a network exists, it is possible to imagine that the sensors in the MPS array could represent nothing more than nodes in this large biofilm network that would probably extend across the length of the system.

In addition to the translational shift of the pattern, once the OCP signals of the upper sensors approach 0 mV, their OCPs began to diverge, even though some of these MPSs were located at the same column height. As illustrated in Video 2, this divergence occurred among the sensors above the 400 mV gradient line, but it also causes this gradient to start dissolving. Interestingly, once almost all OCPs reached $\Delta E < 0$, the sensors below the gradient line started to diverge until each sensor located at the same height position signal differed in OCP. By $t \approx 2300$ h, a new highly disordered gradient emerged, which slowly began to shift toward more positive potentials. Although this behavior could be attributed to diffusive processes occurring over a period of > 1500 h which aimed to reduce the concentration gradient across the three-dimensional space, the difference in OCPs of sensors located at the same height position in the column suggested that the biofilms were actively engaged in influencing the local environment surrounding them. Considering that electrons flow in the presence of an electric potential (voltage gradient), it is reasonable to postulate that the biofilms have mechanisms that generate and modulate these local gradients to enable transfer of electrons and communication across the entire biological network.

When the chamber was capped, the entire system responded to this externally induced change. As shown in Fig. 5, the average OCP of the system decreased. This is evident in Video 2 at $t \approx 2500$ h. Interestingly, the entire array of sensors responded in the same manner; the OCP of all sensors decreased, which shifted the pattern toward lower potentials, yet the pattern shape remained relatively unchanged. In contrast, the ORP probes

did not register this shift in potential or the ORP signal variability was so high that the signal shift was masked as illustrated in Fig. 5(b). Although this figure appears to suggest that there was a relatively good correlation between the ORP and MPS patterns, regression analysis showed that there was no correlation as indicated by $R^2 < 0.1510$ (Fig. SI-3). This lack of correlation between the MPS and ORP sensors became more evident as the system recovered from the "capping" and continued to stabilize. The ORP signals exhibited high fluctuations and variability during this period as illustrated by the 95% confidence intervals in Fig. 5(b). Furthermore, as the MPS signals were relatively stable, the ORP signals started drifting toward more positive values near the end of the experiment. The relative stability of the MPS signals after the system was capped is also illustrated in Video 2. This stability of MPS signals was not unexpected considering that oxygen diffusion was eliminated, and the system had to stabilize at the bio-electrochemical potential dictated by conditions in the sealed column. Beyond oxygen diffusion, this stability of the signals could probably be disturbed by the introduction of other environmental factors like temperature, other favorable electron acceptors like nitrates, or even the presence of photosynthetic organisms, which further increases the monitoring capabilities of the technology.

3.3. *Thermodynamic analysis and implications*

The trends illustrated in Figs. 4 and 5 are consistent with the predictions of thermodynamics for the processes exhibited by these two systems as illustrated in Fig. 6. This figure elucidates the same type of ΔE patterns when the systems were subjected to the same external influences. When high DOC water was added to the system, the total energy of the system increased ($\Delta H_{\text{System}} > 0$) because a "packaged" form of energy was introduced ($\mathrm{d}H = T\mathrm{d}S + V\mathrm{d}P + \Sigma Y_i \mathrm{d}X_i + \Sigma \mu_i \mathrm{d}n_i$ in case of a nonhydrostatic open system, which reduces to $\mathrm{d}H = T\mathrm{d}S + \Sigma \mu_i \mathrm{d}n_i$ under isobaric conditions when also all other relevant generalized coordinates remain constant[55]). The high DOC contains large quantities of reduced carbon forms (e.g., electrons in the high energy bonds), which represents an energy source for the microorganisms to utilize. Consequently, as DOC was added, the Gibbs free energy of the system was increased ($\mathrm{d}G = -S\mathrm{d}T + V\mathrm{d}P + \Sigma Y_i \mathrm{d}X_i + \Sigma \mu_i \mathrm{d}n_i$ in a general case of a nonhydrostatic open system, which reduces to $\mathrm{d}G = \Sigma \mu_i \mathrm{d}n_i$ under isobaric–isothermal conditions when also all other relevant generalized coordinates remain constant[54]). The chemical potentials of individual constituents are increased during this process ($\Delta \mu_i > 0$ when $\Delta a_i > 0$, as $a_i \sim c_i$, where a_i denotes the relative activity of

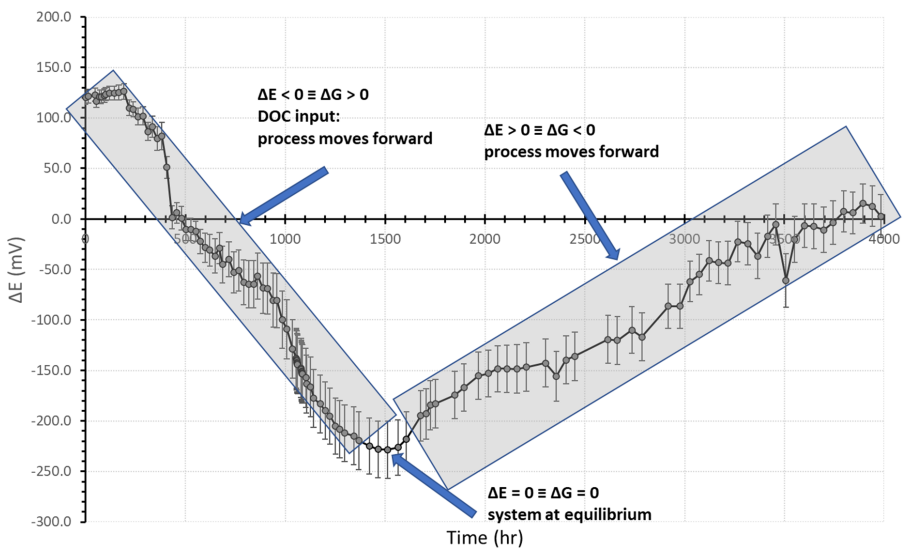

Fig. 6. Thermodynamic predictions for the processes exhibited by the two systems. The gray symbols represent the average OCP signals from the 48 MPS electrodes in chamber 1 for the first 4000 h of monitoring. The error bars represent 95% confidence intervals.

species i in the system). Such chemical potential changes can be later utilized by the microorganisms to do work inside the system. The described change was registered through the drop in the electric potential of the system because $\Delta G = -nF\Delta E$. During the high DOC water injection, the ΔE_{system} over time was decreased ($\Delta E_{\text{system}}/\Delta t < 0$); and considering that $\Delta G = -nF\Delta E$, the change in the Gibbs free energy was also positive ($\Delta G > 0$). Although ΔG was increasing at this stage, the process moved forward because nonequilibrium conditions were induced by "priming" or "energizing" the system with DOC, which introduced new thermodynamic states ($\Delta S = k \ln \Omega$, where k is the Boltzmann constant and Ω is the number of thermodynamic states). The increase in number of new thermodynamic states was probably further facilitated by the biofilm "stripping" the electrons from the absorbed DOC, which resulted in the charging of the temporary electron acceptors (e.g., cytochromes and other similar functional proteins or nanostructures) within the biofilm and causing the MPS electrodes to exhibit drop in ΔE.

Once, however, the external input of high DOC water stopped, the system slowly moved to equilibrium where the change over time in $\Delta E = \Delta G = 0$ as illustrated in Fig. 6. Upon reaching the equilibrium, ΔE_{system} started increasing ($\Delta E > 0$; $\Delta G < 0$) due to the biochemical oxidation of the injected reduced carbon species (respiration), which were enzymatically facilitated by the microorganisms in the system. From open systems thermodynamics, it is known that a process can proceed spontaneously in the "forward" direction under isothermal–isobaric conditions when $\Delta G < 0$ (i.e., $\mathrm{d}G < 0$ considering infinitesimal progressions). Assuming a single biochemical reaction taking place in the system, the total differential of the Gibbs free energy is given by $\mathrm{d}G = -T\mathrm{d}S + V\mathrm{d}P + \Sigma Y_i \mathrm{d}X_{\mathrm{i}} - A\mathrm{d}\xi$, where A denotes the thermodynamic affinity and $\mathrm{d}\xi$ is the change in the reaction extent.[54] As both A and $\mathrm{d}\xi$ are positive for the reaction in progress, under isobaric conditions, assuming also constant values of all relevant generalized coordinates, the expression for $\mathrm{d}G$ acquires the form $\mathrm{d}G = -T\mathrm{d}S - A\mathrm{d}\xi$. If the entropy change occurs solely due to the reaction progress, one can express the first term through $\mathrm{d}\xi$ as well ($\mathrm{d}S = \Delta_r S\, \mathrm{d}\xi$, where $\Delta_r S$ denotes the reaction entropy). So, the expression for $\mathrm{d}G$ reduces to $\mathrm{d}G = -(T\Delta_r S + A)\, \mathrm{d}\xi$. In brief, the essential driving force reduces to the fact that the energy introduced to the systems in the form of reduced carbon is released back into the universe, increasing its entropy.

When high DOC water was introduced at the bottom of the chamber, Video 2 illustrated a very interesting phenomenon. The sensors above the DOC induced ΔE gradient (around the 31st sensor — near the bottom), which were not exposed to high DOC concentrations, simultaneously dropped their OCPs once the pulse reached the gradient. This decrease in OCP appeared not to be induced by the local environment, but somehow was influenced by the sensors at the bottom of the chamber. Considering that the decrease in ΔE is proportional to the increasing entropy of the system, it may appear that the biofilm was trying to minimize the loss of usable energy by dispersing this entropy change across the chamber to the extent the conditions permit. It was also reasonable to postulate that the induced divergence from a stable baseline may be stemming from the same phenomenon; the discrete ΔE of each MPS was affected by the local abilities of a biofilm to disperse the changes in entropy that resulted from the metabolic processes across the entire biofilm network.

Interestingly, however, the changes in Gibbs free energy were not detected by the ORP sensors, except for rapid fluctuations in the ORP signal when the systems were shocked or exited the equilibrium conditions. This finding implied that the ORP electrodes were not capable of monitoring the "packaged" forms of energy introduced into a system unless the redox pairs were in bulk. Considering that the ORP may be considered as the gold standard in monitoring of aquatic environments, this deficiency severely limits their applicability.

4. Conclusions

The findings presented in this study extend beyond the postulated overarching hypothesis that spatial–temporal characterization of contaminant influence redox gradients in a quiescent system could be obtained by creating an MPS array system comprising multiple equidistant biofilm electrodes. The generated data show that the MPS arrays can detect and describe the spatial–temporal changes in an aquatic environment resulting from an influx of carbon rich water, which could

not be detected by conventional ORP electrodes. Interestingly, however, the experiments conducted over a long period of time revealed unusual behaviors. These observed behaviors suggested that biofilms may have an ability to create a large network through which they communicate by means of inducing changes in electric potentials like a sophisticated electronic device. The complex structure of biofilms may be parallel to one of the complex integrated circuits, which comprise transistors, resistors and capacitors. These "biological" circuits within the biofilm could be responsible for the shifts and fluctuations in the electric potentials, resulting from the metabolic processes, in order to create communication mechanisms. Unlike the vessel or other chemical-induced form of communications however, these communication mechanisms appear to be electrical in nature and raise questions on whether biofilms have the ability to disperse changes in entropy or energy. Considering that biofilms exhibit a level of intelligence by the sheer fact that they could chemically or electrically communicate at nano or microdistances, it is rational to postulate that biofilms have evolved the ability to rapidly communicate over long distances (>0.6 m) and distribute energy across their networks like, or potentially better than, more complex multicellular organisms.

Acknowledgment

The authors would like to extend their gratitude to Ms. Michell Peppers for helping with the illustrations and animations.

Conflict of Interest

The corresponding author (K.H.) declares that, as an associate editor of Nano LIFE, there is a conflict of interest regarding this manuscript. However, K.H. confirms that he was not involved in the peer review process of the manuscript, and therefore he has not had any influence on the editorial decision-making process. The conflict of interest was disclosed to the editorial team, and appropriate steps were taken to ensure that the peer review and decision-making process for this manuscript were handled impartially and transparently.

References

1. Z. Lewandowski and H. Beyenal, *Fundamentals of Biofilm Research* (CRC Press, Boca Raton, FL, 2007).
2. K. Sauer, P. Stoodley, D. M. Goeres, L. Hall-Stoodley, M. Burmølle, P. S. Steward and T. Bjarnsholt, *Nat. Rev. Microbiol.* **20**, 608 (2022).
3. H.-C. Flemming, E. D. van Hullebuch, T. R. Neu, P. H. Nielsen, T. Seviour, P. Stoodley, J. Wingender and S. Wuertz, *Nat. Rev. Microbiol.* **21**, 70 (2022).
4. A. Penesyan, I. T. Paulsen, S. Kjelleberg and M. R. Gillings, *NPJ Biofilms Microbiomes* **7**, 80 (2021).
5. R. M. Donlan, *EID J.* **8**, 881 (2002).
6. A. Prindle, J. Liu, M. Asally, S. Ly, J. Garcia-Ojalvo and G. M. Süel, *Nature* **527**, 59 (2015).
7. R. Martinez-Corral, J. Liu, A. Prindle, G. M. Süel and J. Garcia-Ojalvo, *Philos. Trans. R. Soc. Lond. B Biol. Sci.* **374**, 1774 (2019).
8. S. Manna, C. Ghanty, P. Baindara, T. Kr. Barik and S. M. Mandal, *J. Basic Microbiol.* **60**, 819 (2020).
9. K. Rabbaey, N. Boon, S. D. Siciliano, M. Verhaege and W. Verstraete, *Appl. Environ. Microb.* **70**, 5373 (2004).
10. I. S. Chang, H. Moon, O. Bretschger, J. K. Jang, H. I. Park, K. H. Nealson and B. H. Kim, *J. Microbiol. Biotechnol.* **16**, 163 (2006).
11. A. Dewan, H. Beyenal and Z. Lewandowski, *Environ. Sci. Technol.* **42**, 7643 (2008).
12. A. E. Franks, K. P. Nevin, H. F. Jia, M. Izallalen, T. L. Woodard and D. R. Lovley, *Energ. Environ. Sci.* **2**, 113 (2009).
13. N. S. Malvankar, M. Vargas, K. P. Nevin, A. E. Franks, C. Leang, B. C. Kim, K. Inoue, T. Mester, S. F. Covalla, J. P. Johnson, V. M. Rotello, M. T. Tuominen and D. R. Lovley, *Nat. Nanotechnol.* **6**, 573 (2011).
14. J. Babauta, R. Renslow, Z. Lewandowski and H. Beyenal, *Biofouling* **28**, 789 (2012).
15. E. Marsili, D. B. Baron, I. D. Shikhare, D. Coursolle, J. A. Gralnick and D. R. Bond, *Proc. Natl. Acad. Sci. USA* **105**, 3968 (2008).
16. B. Erable, D. Feron and A. Bergel, *ChemSusChem* **5**, 975 (2012).
17. D. R. Bond and D. R. Lovley, *Appl. Environ. Microb.* **69**, 1548 (2003).
18. F. Mansfeld, *Electrochim. Acta* **52**, 7670 (2007).
19. H. Richter, K. McCarthy, K. P. Nevin, J. P. Johnson, V. M. Rotello and R. D. Lovley, *Langmuir* **24**, 4376 (2008).
20. Y. Liu, H. Kim, R. R. Franklin and D. R. Bond, *Chem. Phys. Chem.* **12**, 2235 (2011).
21. J. P. Busalmen, A. Esteve-Nunez, A. Berna and J. M. Feliu, *Bioelectrochemistry* **78**, 25 (2010).
22. J. T. Babauta, Electron Transfer mechanisms in electrochemically active biofilms, Ph.D. Thesis, Washington State University (2012).
23. X. Zhang, Extracellular electron transport of electroactive biofilm, *Bioelectrosynthesis: Principles and Technologies for Value-Added Products*, eds. A.

Wang, W. Liu, B. Zhang and W. Cai (Wiley, 2020), pp. 295–305.
24. L. Zou, F. Zhu, Z. Long and Y. Huang, *J. Nanobiotechnol.* **19**, 120 (2021).
25. E. M. Conners, K. Rengasamy and A. Bose, *J. Ind. Microbiol. Biotechnol.* **49**, 1 (2022).
26. G. S. Jadhav and M. M. Ghangrekar, *Bioresource Technol.* **100**, 717 (2009).
27. K. P. Katuri, P. Kavanagh, S. Rengaraj and D. Leech, *Chem. Commun.* **46**, 4758 (2010).
28. T. Yu and L. P. Bishop, *Water Sci. Technol.* **37**, 195 (1998).
29. J. S. McLean, G. Wanger, Y. A. Gorby, M. Wainstein, J. McQuaid, S. I. Ishii, O. Bretschger, H. Beyenal and K. H. Nealson, *Environ. Sci. Technol.* **44**, 2721 (2010).
30. J. S. McLean, P. D. Majors, C. L. Reardon, C. L. Bilskis, S. B. Reed, M. F. Romine and J. K. Fredrickson, *J. Microbiol. Methods* **74**, 47 (2008).
31. J. T. Babauta, H. D. Nguyen and H. Beyenal, *Environ. Sci. Technol.* **45**, 6654 (2011).
32. A. P. Borole, D. Aaron, C. Y. Hamilton and C. Tsouris, *Environ. Sci. Technol.* **44**, 2740 (2010).
33. A. K. Manohar, O. Bretschger, K. H. Nealson and F. Mansfeld, *Bioelectrochemistry* **72**, 149 (2008).
34. K. B. Oldham and J. C. Myland, *Fundamentals of Electrochemical Science* (Academic Press, San Diego, 1994).
35. S. Srikanth, S. V. Mohan and P. N. Sarma, *Bioresource Technol.* **101**, 5337 (2010).
36. A. Larossa-Guerrero, K. Scott, K. P. Katuri, C. Godinez, I. M. Head and T. Curtis, *Appl. Microbiol. Biot.* **87**, 1699 (2010).
37. D. N. Myers, Water-quality sensors with case studies on floods, hurricanes, and harmful algal blooms, *Evaluating Water Quality to Prevent Future Disasters*, ed. S. Ahuja (Elsevier Inc., 2019), pp. 219–283.
38. S. A. Burge, K. D. Hristovski, R. S. Burge, D. A. Hoffman, D. Saboe, P. Chao, E. Taylor and S. S. Koenigsberg, *Sci. Total Environ.* **742**, 140528 (2020).
39. T. Sale, S. Gallo, K. K. Askarani, M. Irianni-Renno, M. Lyverse, H. Hopkins, J. Blotevogel and S. Burge, *J. Hazard. Mater.* **408**, 124403 (2021).
40. R. N. Glud, N. B. Ramsing and N. P. Revsbech, *J. Phycol.* **28**, 51 (1992).
41. T. C. Zhang and P. L. Bishop, *Water Sci. Technol.* **30**, 47 (1994).
42. R. Renslow, C. Donovan, M. Shim, J. Babauta, S. Nannapaneni, J. Schenk and H. Beyenal, *Phys. Chem. Chem. Phys.* **13**, 21573 (2011).
43. S. R. Burge, K. D. Hristovski, R. G. Burge, D. Saboe, D. A. Hoffman and S. S. Koenigsberg, *Sci. Total Environ.* **751**, 142342 (2021).
44. F. C. Brown, S. R. Burge, K. D. Hristovski, R. G. Burge, E. Taylor and D. A. Hoffman, *Maced. J. Chem. Chem. Eng.* **39**, 119 (2020).
45. D. Saboe, H. Ghasemi, M. M. Gao, M. Samardzic, K. D. Hristovski, D. Boscovic, S. R. Burge, R. G. Burge and D. A. Hoffman, *Sci. Total Environ.* **764**, 142876 (2021).
46. D. Saboe, K. D. Hristovski, S. R. Burge, R. G. Burge, E. Taylor and D. A. Hoffman, *Sci. Total Environ.* **766**, 144424 (2021).
47. K. D. Hristovski, S. R. Burge, D. Boscovic, R. G. Burge and F. Babanovska-Milenkovska, *J. Environ. Chem. Eng.* **10**, 107491 (2022).
48. S. N. Yang and Z. Lewandowski, *Biotechnol. Bioeng.* **48**, 737 (1995).
49. F. H. Xia, H. Beyenal and Z. Lewandowski, *Water Res.* **32**, 3631 (1998).
50. H. Beyenal and Z. Lewandowski, *Water Res.* **34**, 528 (2000).
51. C. C. H. Cronenberg and J. C. Vandenheuvel, *Biosens. Bioelectron.* **6**, 255 (1991).
52. H. Beyenal and Z. Lewandowski, *Biotechnol. Progr.* **18**, 55 (2002).
53. H. Beyenal and Z. Lewandowski, *Aiche J.* **47**, 1689 (2001).
54. H. Beyenal, A. Tanyolac and Z. Lewandowski, *Water Sci. Technol.* **38**, 171 (1998).
55. E. Keszei, *Chemical Thermodynamics* (Springer-Verlag, Berlin Heidelberg, 2012).